Stem Cell Reports
Article

ISSCR

OPEN ACCESS

Increased Calcium Influx through L-type Calcium Channels in Human and Mouse Neural Progenitors Lacking Fragile X Mental Retardation Protein

Claudia Danesi,[1] Venkat Swaroop Achuta,[1] Padraic Corcoran,[2] Ulla-Kaisa Peteri,[1] Giorgio Turconi,[1] Nobuaki Matsui,[3] Ilyas Albayrak,[1] Veronika Rezov,[1] Anders Isaksson,[2] and Maija L. Castrén[1,*]

[1]Faculty of Medicine, Physiology, University of Helsinki, PO Box 63, FIN-00014 University of Helsinki, Helsinki, Finland
[2]Array and Analysis Facility, Department of Medical Sciences, Uppsala University, PO Box 3056, 75003 Uppsala, Sweden
[3]Department of Pharmacology, Faculty of Pharmaceutical Sciences, Tokushima Bunri University, Tokushima, 770-8514, Japan
*Correspondence: maija.castren@helsinki.fi
https://doi.org/10.1016/j.stemcr.2018.11.003

SUMMARY

The absence of FMR1 protein (FMRP) causes fragile X syndrome (FXS) and disturbed FMRP function is implicated in several forms of human psychopathology. We show that intracellular calcium responses to depolarization are augmented in neural progenitors derived from human induced pluripotent stem cells and mouse brain with FXS. Increased calcium influx via nifedipine-sensitive voltage-gated calcium (Ca_v) channels contributes to the exaggerated responses to depolarization and type 1 metabotropic glutamate receptor activation. The ratio of L-type/T-type Ca_v channel expression is increased in FXS progenitors and correlates with enhanced progenitor differentiation to glutamate-responsive cells. Genetic reduction of brain-derived neurotrophic factor in FXS mouse progenitors diminishes the expression of Ca_v channels and activity-dependent responses, which are associated with increased phosphorylation of the phospholipase C-γ1 site within TrkB receptors and changes of differentiating progenitor subpopulations. Our results show developmental effects of increased calcium influx via L-type Ca_v channels in FXS neural progenitors.

INTRODUCTION

Monogenic disorders such as fragile X syndrome (FXS) are useful for studies that investigate defective molecular pathways in intellectual disability syndromes. FXS results from the absence of fragile X mental retardation protein (FMRP), which is caused by a CGG triplet repeat expansion leading to transcriptional silencing of the *FMR1* gene (Verkerk et al., 1991). FMRP is an RNA-binding protein that is important for translational regulation of many brain mRNAs (Darnell et al., 2011). FMRP is necessary for normal brain development and formation of functional neuronal connections (Contractor et al., 2015). The behavioral phenotype of FXS includes cognitive impairment, defective communication, abnormal sensory reactivity, anxiety, hyperactivity, gaze aversion, and impulsivity (Lozano et al., 2014). The main phenotype and molecular findings in human FXS are recapitulated in *Fmr1* knockout (KO) mice (Kooy et al., 1996). Altered neuronal differentiation and migration disrupt formation of cortical layers in the *Fmr1* KO mouse brain and affect developmental processes involved in neuronal circuit formation and function (Gonçalves et al., 2013; La Fata et al., 2014; Tervonen et al., 2009).

Ca^{2+}-mediated signals regulate many processes during neuronal development, including progenitor proliferation, neuronal migration and differentiation, axon guidance, and dendrite growth (Rosenberg and Spitzer, 2011; Zheng and Poo, 2007). Several forms of Ca^{2+} activity take place during cortical development and are mediated by metabotropic glutamate receptors (mGluRs), gap junctions, GABAa receptors, and ionotropic glutamate receptors (iGluRs). Voltage-gated calcium (Ca_v) channels are the major source of Ca^{2+} influx in electrically excitable cells and have a great impact on cell signaling (Rosenberg and Spitzer, 2011). Three subfamilies of Ca_v channels have been identified (Ca_v1-3); L-type calcium (Ca_v1) channels represent one of the major classes of Ca_v channels (Dolphin, 2016). Ca_v1 channels are subdivided into four isoforms (Ca_v1.1, Ca_v1.2, Ca_v1.3, and Ca_v1.4) based on the pore-forming α1 subunit that selectively conducts calcium ions. Ca_v1.2 and Ca_v1.3 (encoded by the *Cacna1c* and *Cacna1d* genes, respectively) are the predominant subunits of the L-type Ca_v channels in the brain and are expressed in neural progenitor cells (NPCs) (Louhivuori et al., 2013). Treatment with Ca_v1 blockers inhibits functional maturation of neurons (D'Ascenzo et al., 2006) and reduces dendritic outgrowth and synapse formation in murine NPC cultures (Lepski et al., 2013).

FXS neurons differentiated *in vitro* from human pluripotent stem cells, and cultured from *Fmr1* KO mouse brain show abnormal maturation and functional deficits (Boland et al., 2017; Braun and Segal, 2000; Telias et al., 2015). In both human and mouse FXS NPCs, aberrant functional responses are detectable already at the very early stages of neuronal differentiation (Achuta et al., 2017, 2018), and augmented activity-dependent intracellular calcium responses are consistent with increased neuronal excitability in FXS (Achuta et al., 2014; Louhivuori et al., 2011). Here we studied the contribution of L-type Ca_v channels to the

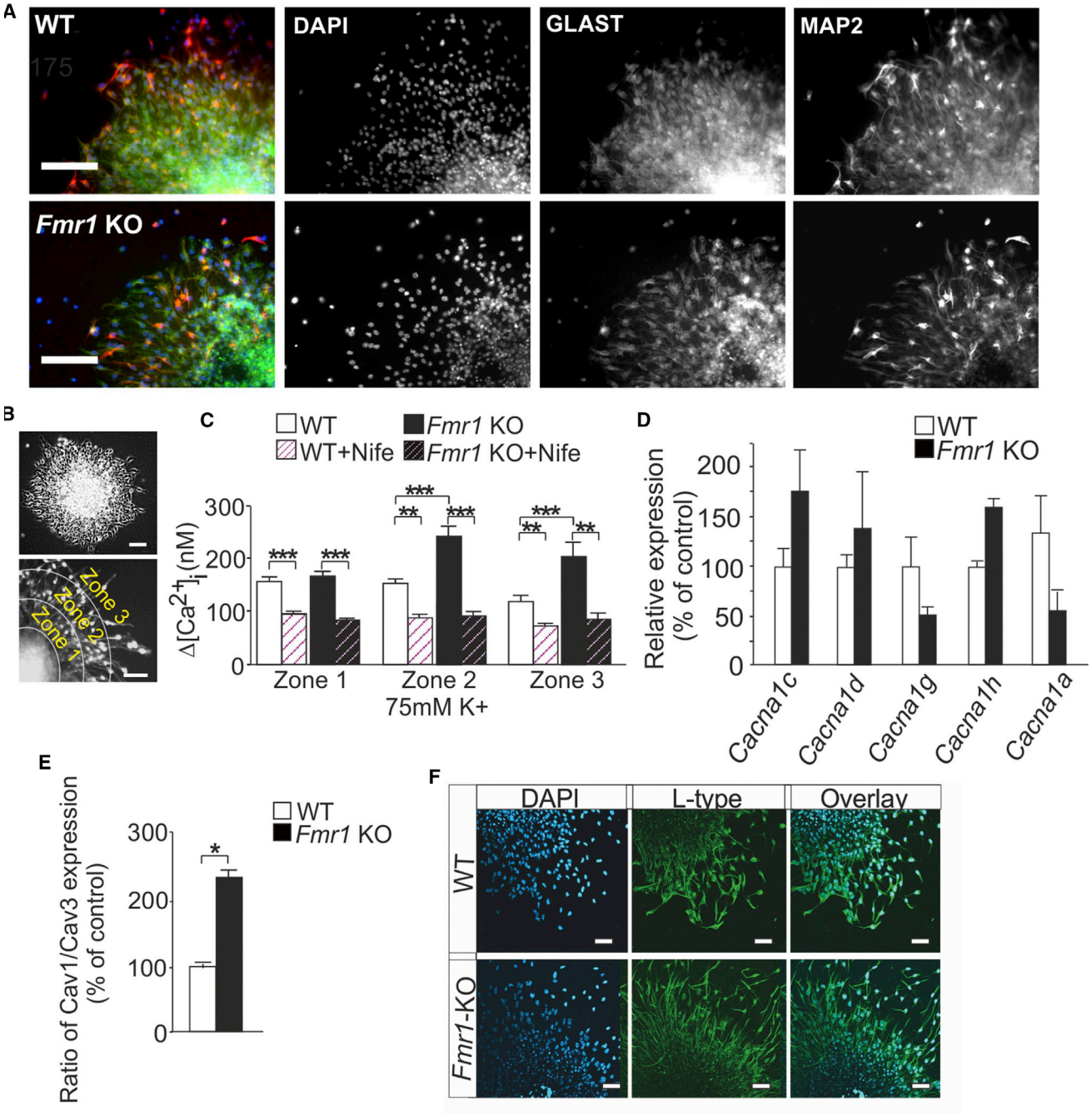

Figure 1. Intracellular Calcium Responses via L-type Voltage-Gated Calcium Channels and Expression of Channel Subunits in Mouse NPCs Lacking FMRP

(A) Representative images of WT and *Fmr1* KO mouse neurospheres immunostained for GLAST (green) and MAP2 (red) at day 1 of differentiation. Scale bars, 100 μm.

(B) A bright-field image of a neurosphere and a Fura-2 fluorescence image showing the migration area that was categorized into three zones (zones 1–3). Scale bars, 100 μm.

(C) Average amplitude of $[Ca^{2+}]_i$ response in differentiated cells of WT and *Fmr1* KO mouse neurospheres after stimulation with high (75 mM) $[K^+]_e$ and effects of nifedipine (nife) on $[K^+]_e$-evoked responses. WT(n) = 8, *Fmr1* KO(n) = 8, WT + nife(n) = 4, and *Fmr1* KO + nife(n) = 4 neurospheres; responses of 75–100 cells were measured in each experiment.

(legend continued on next page)

differentiation defects of NPCs derived from human induced pluripotent stem cells (iPSCs) and mouse brain with FXS. Our results demonstrate a central role for increased Ca^{2+} influx through L-type Ca_v channels in augmented responses to activity, altered fate determination of neuronal cells, and migration defect of FXS NPCs.

RESULTS

Augmented Intracellular Calcium Responses via L-type Ca_v Channels in Mouse FMRP-Deficient NPCs

Depolarization with high extracellular potassium ($[K^+]_e$) results in augmented intracellular calcium ($[Ca^{2+}]_i$) responses in differentiating NPCs generated from *Fmr1* KO mice compared with wild-type (WT) controls (Achuta et al., 2014). Differentiating NPCs express functional Ca_v channels that mediate Ca^{2+} influx in response to membrane depolarization (D'Ascenzo et al., 2006). We studied the contribution of L-type Ca_v channels to the increased Ca^{2+} entry to mouse cortical progenitors lacking FMRP by investigating the effects of nifedipine (a blocker of L-type Ca_v channels) on $[Ca^{2+}]_i$ responses in *Fmr1* KO neurospheres. We induced NPC differentiation by withdrawal of mitogens and monitored $[Ca^{2+}]_i$ responses in all or most differentiated cells migrated out from the neurosphere (Figures 1A and 1B). The migration area was divided into three zones to analyze the functional responses in differentially migrated cells (Figure 1B). Nifedipine blocked the $[Ca^{2+}]_i$ responses elicited by depolarization with 75 mM $[K^+]_e$ in FMRP-deficient NPCs to the levels of nifedipine-treated WT cells in the whole migration area (Figure 1C), indicating that Ca^{2+} influx into FMRP-deficient cells was abnormally increased through Ca_v1 channels.

Ca_v channels are heteromultimers composed of a pore-forming α1 subunit and auxiliary β and $\alpha_2\delta$ subunits (Dolphin, 2016). All Ca_v channel α1 subunits were expressed at low levels and showed high variation in NPCs grown in neurospheres. Detectable amounts of mRNAs allowed analysis of the expression of *Cacna1c* and *Cacna1d* for L-type-specific α1 subunits, *Cacna1g* and *Cacna1h* for T-type α subunits, and *Cacna1a* for P/Q-type α subunits. Although *Cacna1c* and *Cacna1d* expression showed a tendency to be increased in FMRP-deficient mouse NPCs compared with controls, we found no significant differences of any α1 subunit expression between WT and *Fmr1* KO NPCs (Figure 1D). However, the ratio of the L-type/T-type α1 subunit mRNA expression was 5.1-fold higher in undifferentiated *Fmr1* KO neurospheres and 2.3-fold higher in FMRP-deficient NPCs compared with WT controls at day 1 of differentiation (Figure 1E). As shown in Figure 1F, the protein expression of the L-type channel α1 subunits did not differ between *Fmr1* KO and WT NPCs at the single-cell level, indicating changes in the differentiated subpopulations of cells and enhanced differentiation of NPCs expressing L-type channels in the absence of FMRP.

Augmented Single-Cell Responses to Membrane Depolarization in Human FXS iPSC-Derived NPCs

As in mouse FXS NPCs, responses to membrane depolarization by increased $[K^+]_e$ were higher (2.1-fold) in human FXS iPSC-derived NPCs than in controls (Figure 2A). We found that the relative *CACNA1G* expression was reduced (Figure 2B), while the *CACNA1C* expression was not affected (data not shown) in FXS NPCs at day 1 of differentiation relative to that of undifferentiated NPCs in the transcriptome analysis of NPCs derived from three control and three FXS iPSC lines. The expression of the Ca_v channel α1 subunits showed very high variability between cell lines and we found no significant differences in the expression of the α1 subunits between FXS and control NPCs (Figure 2C). The results of both human and mouse FXS NPCs suggested that the expression of T-type Ca_v channels was switched to L-type channels and correlated with enhanced NPC differentiation to glutamate-responsive cells in FXS NPCs.

We analyzed the transcriptome data of human iPSC-derived NPCs to identify Ca^{2+}regulated pathways that associate with the augmented Ca_v1 responses in FXS NPCs. In this respect, only one significant change was identified; in the splicing-specific transcriptome analysis the *CAST* gene expression was altered in FXS NPCs. The *CAST* gene encodes calpastatin, which can regulate L-type Ca_v function directly or as a natural inhibitor of calpains. We found an alternative splicing event leading to exon skipping in the *CAST* gene in FXS NPCs (Figure 2D). The probe set, including both exon and exon junction probes, detected an alternative splicing event ($p = 0.026$) in chromosome 5 at the genome location 96740745–96740783 (ENSE00003628178). Exon 19 encoding 39 base pairs of the *CAST* gene was removed in FXS NPCs. This exon encodes part of the calpastatin protein and its differential splicing has not previously been reported.

(D and E) The relative mRNA expression of *Cacna1c*, *Cacna1d*, *Cacna1g*, *Cacna1h*, and *Cacna1a* in WT and *Fmr1* KO neurospheres (D) and the L-type Ca_v channel/T-type Ca_v channel expression ratio in NPCs at day 1 of differentiation (E). Each group(n) = 4–5 in twice repeated experiment.

(F) Immunofluorescent images showing L-type Ca_v channel α_{1c} subunit expression (green) in WT and *Fmr1* KO NPCs differentiated for 1 day. Data are expressed as means ± SEM; ***$p < 0.001$, **$p < 0.01$, *$p < 0.05$.

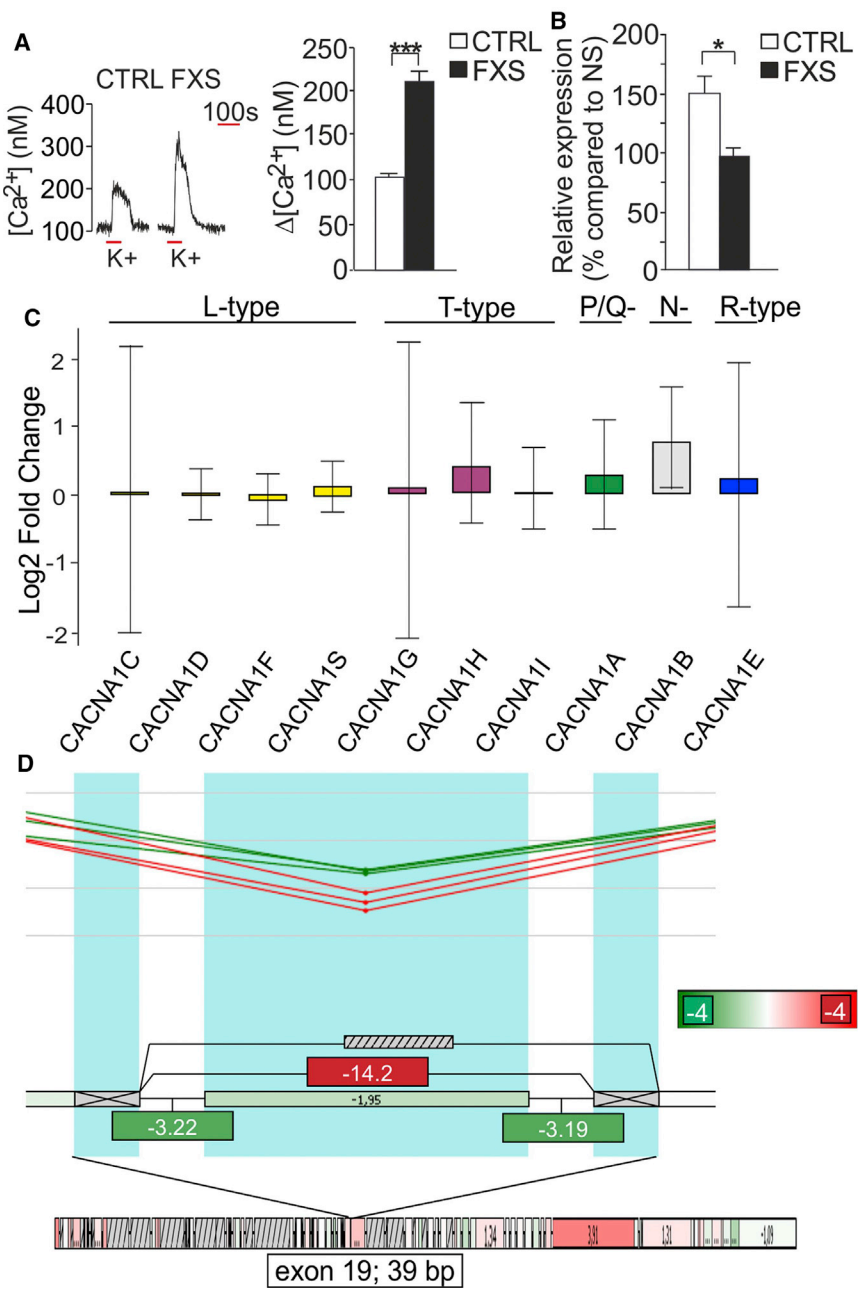

Figure 2. Augmented Intracellular Ca^{2+} Responses to Depolarization and the Expression of Ca_v Channels and a Splicing Defect of the CAST Gene in Human FXS NPCs

(A) Representative single-cell responses to high $[K^+]_e$ and average amplitude of $[Ca^{2+}]_i$ responses in human FXS and control (CTRL) NPCs. Data are from n(CTRL) = 5 and n(FXS) = 6 neurospheres. HEL46.11, HEL11.4, HEL100.1, HEL100.2, and HEL70.3 cell lines; responses of 50–100 cells were measured in each neurosphere.

(B) Relative *CACNA1G* expression in NPCs at day 1 of differentiation compared with that in undifferentiated FXS and control neurospheres (NS).

(C) mRNA expression of the pore-forming α1 subunits of Ca_v channels in human FXS and control NPCs. n(CTRL) = 3 cell lines (HEL11.4, HEL23.3, and HEL46.11) and n(FXS) = 3 cell lines (HEL69.5, HEL70.3, and HEL10.2).

(D) Schematic presentation of the alternative splicing of the *CAST* gene in FXS NPCs. Splicing index of the exon and junction probe set is shown; splicing index 18.35 correlates with a 21.06-fold change; event pointer $p < 0.05$.

Data are expressed as means ± SEM; ***$p < 0.001$, *$p < 0.05$ by Student's t test.

Genetic Reduction of BDNF Expression Prevents Augmentation of Activity-Dependent Responses in FMRP-Deficient NPCs

Ca_v channel-mediated elevation of Ca^{2+} levels triggers transcription of the *Bdnf* gene (Zheng et al., 2011) and the increased activation of Ca_v1 channels in FMRP-deficient NPCs correlates with the upregulated expression of brain-derived neurotrophic factor (BDNF) mRNAs shown previously in undifferentiated FXS mouse NPCs (Uutela et al., 2014). BDNF mRNA expression is also increased and regulated in an activity-dependent manner in mouse FMRP-deficient neurons *in vitro* and *in vivo*, but in *Fmr1* KO neurospheres, reduced differentiation of cells expressing BDNF modulates total BDNF mRNA and protein expression (Louhivuori et al., 2011). In human iPSC-derived NPCs, BDNF mRNA expression showed high variation and did not differ significantly between FXS and control NPCs at the early stage of differentiation (Figure 3A). To explore effects of BDNF on aberrances of FXS NPC differentiation we investigated the differentiation of BDNF-deficient FXS NPCs derived from dMT mice (Uutela et al., 2012). BDNF protein expression was reduced by 50% in dMT NPCs compared

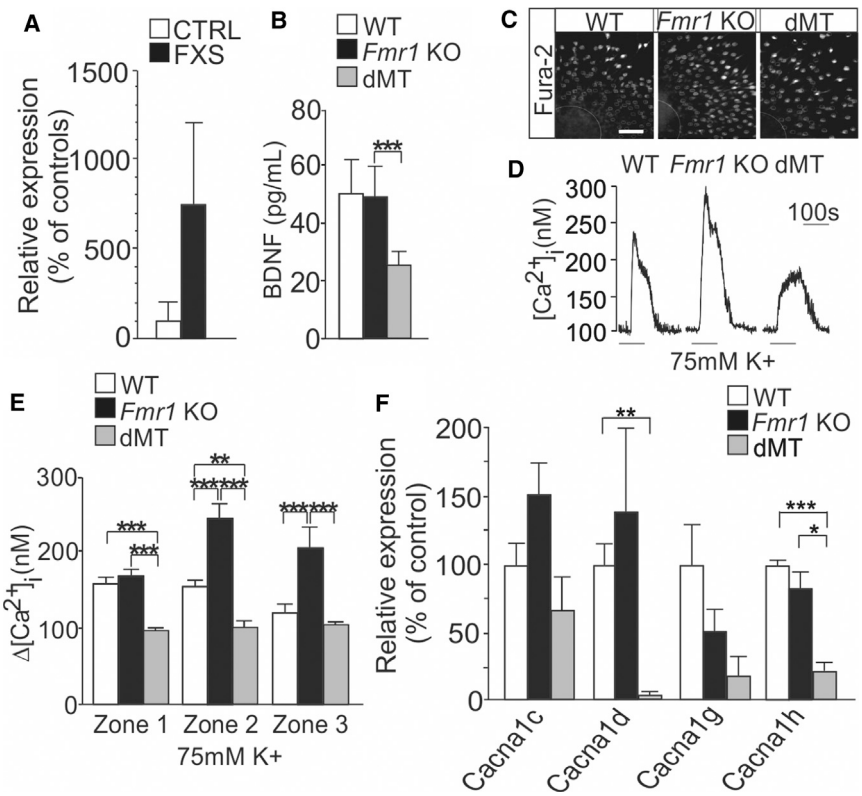

Figure 3. Effects of Reduced BDNF Expression on Augmented Responses to Activity in FXS NPCs

(A) *BDNF* mRNA expression in human iPSC-derived progenitors at day 1 of differentiation. CTRL(n) = 3 cell lines (HEL11.4, HEL23.3, and HEL46.11) and FXS(n) = 3 cell lines (HEL69.5, HEL70.3, and HEL10.2).

(B) BDNF protein expression in neurospheres derived from WT, *Fmr1* KO, and dMT mouse brain. Data are from three cultures of each experimental group.

(C) Fura-2 images showing migration area of WT, *Fmr1* KO, and dMT neurospheres. Scale bars, 100 μm.

(D) Representative single-cell response after stimulation with 75 mM $[K^+]_e$ in WT, *Fmr1* KO, and dMT NPCs during the period indicated.

(E) Average amplitude of $[Ca^{2+}]_i$ in cells in three zones of the migration area of WT, *Fmr1* KO, and dMT neurospheres after depolarization with 75 mM $[K^+]_e$. WT(n) = 8, *Fmr1* KO(n) = 8, and dMT(n) = 7 neurospheres; responses of 75–100 cells were measured in each experiment.

(F) The relative mRNA expression of *Cacna1c*, *Cacna1d*, *Cacna1g*, and *Cacna1h* in dMT NPCs compared with WT and *Fmr1* KO mouse NPCs at day 1 of differentiation. Each group(n) = 4–5 in twice repeated experiments.

Data are expressed as means ± SEM; ***$p < 0.001$, **$p < 0.01$, and *$p < 0.05$, one-way ANOVA with Tukey *post hoc* test.

with that in WT and *Fmr1* KO NPCs (Figure 3B). We found that the amplitude of $[Ca^{2+}]_i$ responses to high $[K^+]_e$ was reduced in dMT NPCs compared with that in *Fmr1* KO NPCs at days 1 (Figures 3C–3E) and 7 of differentiation (data not shown). Expression of both L- and T-type Ca_v channels was reduced in dMT NPCs; the expression of *Cacna1h* was reduced versus *Fmr1* KO and control NPCs and the expression of *Cacna1d* versus controls (Figure 3F).

Increased Ca^{2+} Influx Augments Responses to Type I mGluR Activation in FMRP-Deficient NPCs

Overactive or inappropriate signaling via the type I mGluRs is implicated as the key mechanism in the pathophysiology of FXS (Huber et al., 2002). Our previous studies showed that $[Ca^{2+}]_i$ responses to (S)-3,5-dihydroxyphenylglycine (DHPG), a specific agonist of type I mGluRs, are augmented in FXS NPCs (Achuta et al., 2017) and that FXS NPCs give rise to abnormally high amounts of cells expressing Ca^{2+}-permeable AMPA receptors (Achuta et al., 2018), which could facilitate mGluR5-signaling via L-type Ca_v channels (Kim et al., 2015). DHPG stimulation induced robust sustained $[Ca^{2+}]_i$ responses in cells correlating with radial glial cells in differentiating mouse NPCs (Figure 4A). The amplitude of DHPG responses was decreased in dMT NPCs below WT levels at days 1 and 7 of differentiation in the presence of extracellular calcium ($[Ca^{2+}]_e$) (Figures 4A and 4B). When $[Ca^{2+}]_e$ was removed, DHPG induced only a transient $[Ca^{2+}]_i$ rise (Figure 4C), and the average amplitude of DHPG responses did not differ in *Fmr1* KO, WT, and dMT NPCs (Figures 4C and 4D). The data indicated that the DHPG-induced $[Ca^{2+}]_i$ increase in *Fmr1* KO NPCs was primarily caused by increased Ca^{2+} influx and reduced BDNF dampened DHPG responses by affecting Ca^{2+} entry into cells. The effects were specific to mGluR signaling, and the magnitude of $[Ca^{2+}]_i$ responses to kainic acid (KA) or N-methyl-D-aspartate (NMDA) did not differ in WT, *Fmr1* KO, and dMT progenitors (Figures 4E and 4F).

Reduced BDNF Deceases Ca_v Channel Expression and Alters Progenitor Mobility and Differentiation in FMRP-Deficient Neurospheres

Having established a role for BDNF in increased Ca_v1 channel activity in FMRP-deficient NPCs, we examined the effects of reduced BDNF on the previously reported enhanced differentiation and motility of FXS NPCs (Achuta et al., 2017). We found that the enhanced progenitor differentiation to glutamate-responsive cells characteristic of FXS NPCs was normalized in dMT neurospheres.

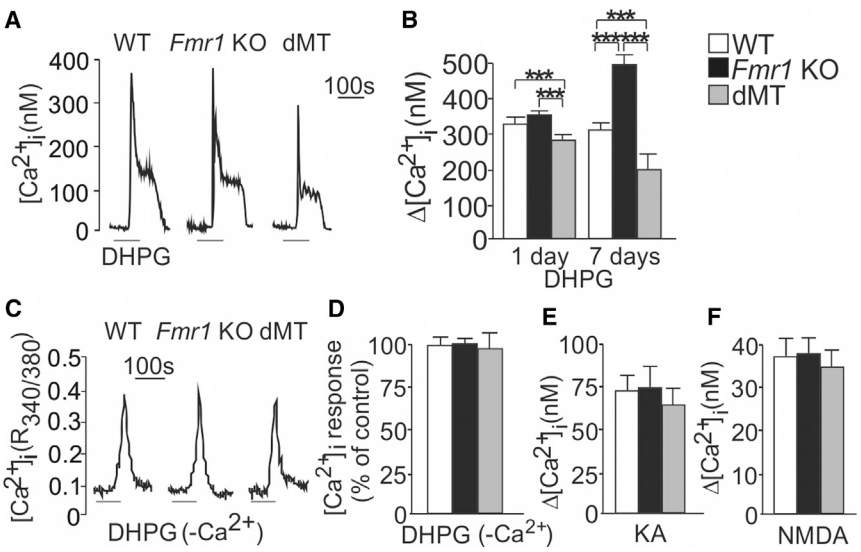

Figure 4. Effects of Extracellular Ca^{2+} and Reduced BDNF on Intracellular Ca^{2+} Responses in FMRP-Deficient NPCs

(A and B) Representative single-cell response (A) and average amplitude of $[Ca^{2+}]_i$ responses to DHPG in the presence of $[Ca^{2+}]_e$ in WT, *Fmr1* KO, and dMT NPCs at day 1 and 7 of differentiation (B).

(C–F) Representative single-cell response (C) and average amplitude of $[Ca^{2+}]_i$ responses to DHPG in the absence of $[Ca^{2+}]_e$ in WT, *Fmr1* KO, and dMT neurospheres at day 7 of differentiation (D). Average Ca^{2+}amplitude of responses in WT, *Fmr1* KO, and dMT NPCs (E) to kainate (KA) and (F) to NMDA at day 7 of differentiation. WT(n) = 6, *Fmr1* KO(n) = 8, and dMT(n) = 5 neurospheres at day 1; WT(n) = 3–5, *Fmr1* KO(n) = 3–5, and dMT(n) = 3–5 neurospheres at day 7; responses of 75–100 cells were measured in each experiment. Data are expressed as means ± SEM. ***p < 0.001, one-way ANOVA with Tukey *post hoc* test.

The proportion of cells responsive to glutamate agonists (DHPG/KA/NMDA) was reduced in dMT NPCs to WT levels at days 1 and 7 of differentiation (Figure 5A). We also investigated the migration of NPCs by monitoring the motility of freely moving neuron-like cells that appear at the outer border of the migration area during the first 24 hr of differentiation by time-lapse imaging (Figure 5B). Images of cells migrating out from the neurospheres were taken every 15 min. We observed that the freely moving cells migrated with a higher velocity in *Fmr1* KO neurospheres than in WT neurospheres during 12–24 hr of differentiation and that the mean velocity was normalized in dMT NPCs (Figure 5C). A detailed analysis revealed that the velocity was particularly affected in FMRP-deficient NPCs during 12–18 hr (Figure 5D), when reduced BDNF expression normalized the motility of cells by decreasing the ratio of fast (surges) and slow (stalling) motility phases in dMT neurospheres to WT levels (Figure 5E). The results are consistent with the previous report showing that BDNF modulates the phasic motility of differentiating neuron-like cells during neurosphere differentiation by promoting the initiation and maintenance of phases of cell motility (Jansson et al., 2012).

The proportion of all DHPG-responsive progenitors was smaller in dMT neurospheres than that in *Fmr1* KO and WT neurospheres in the presence of $[Ca^{2+}]_e$ (Figure 5F). When $[Ca^{2+}]_e$ was removed, the increased proportion of DHPG-responsive NPCs in *Fmr1* KO neurospheres (Castrén et al., 2005) was normalized to WT levels in dMT neurospheres (Figure 5G). Finally, the proportion of cells responsive to KA or NMDA without DHPG responses was further increased from the abnormally high *Fmr1* KO levels in dMT NPCs (Figures 5H–5J). Altogether, the data are in agreement with a special role of BDNF-mediated calcium dynamics in the differentiation of distinct subsets of NPCs (Louhivuori et al., 2011).

Increased Phosphorylation of TrkB Receptors in Fmr1 KO NPCs with the Genetic Deletion of BDNF

We found that the phosphorylation of the phospholipase-Cγ1 (PLCγ1)-binding tyrosine within TrkB receptors ($TrkB^{y816}$) was increased in undifferentiated dMT NPCs when normalized with total TrkB expression and compared with that of *Fmr1* KO NPCs (Figures 6A–6C). We did not detect any increase in the TrkB phosphorylation within the other phosphorylation sites (Figure S1), suggesting that reduced BDNF expression regulated specifically the PLC-γ1 signaling in FXS NPCs. Indeed, Ca_v1 channel antagonist nimodipine has been shown to specially increase neuronal TrkB phosphorylation of the PLCγ1 domain in the mouse prefrontal cortex and hippocampus (Koskimäki et al., 2015). Thus, studies of dMT NPCs revealed the link between dysregulated dihydropyridine-sensitive Ca_v channels and $TrkB^{y816}$ phosphorylation in NPCs lacking FMRP.

DISCUSSION

Calcium signaling is implicated in the regulation of neuronal differentiation, migration, and survival (Platel et al., 2008; Rosenberg and Spitzer, 2011). Ca^{2+} influx

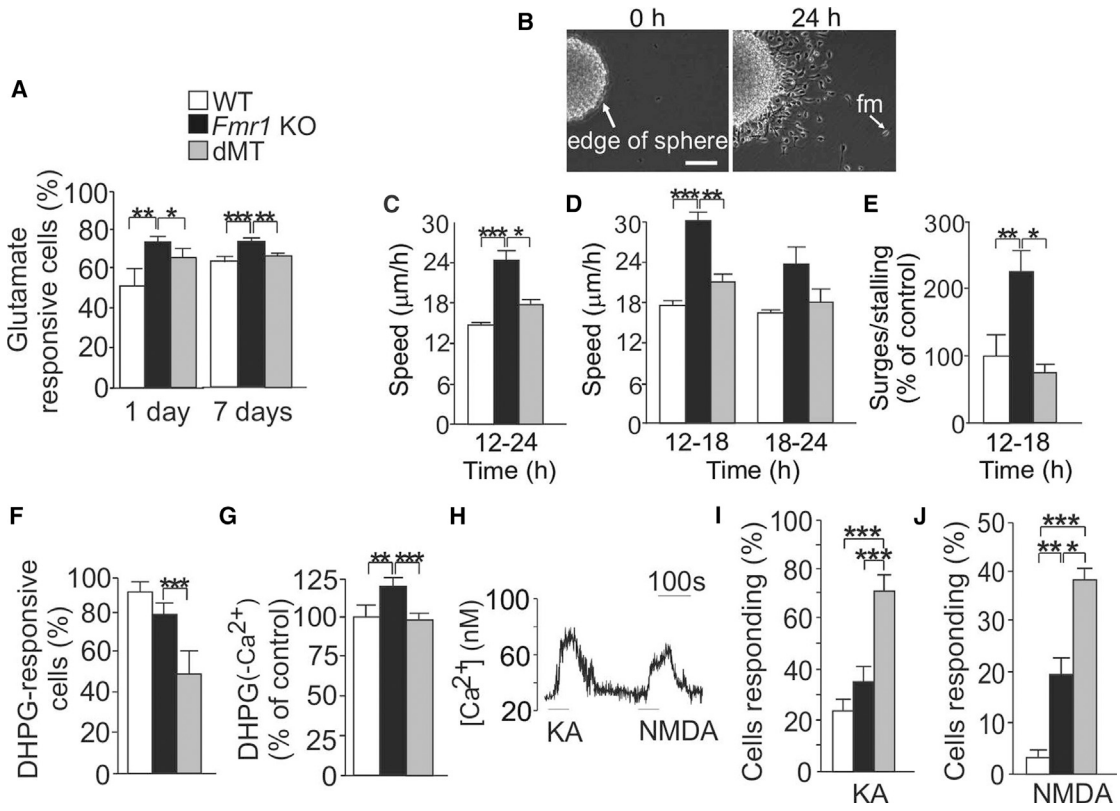

Figure 5. Effects of Reduced BDNF on the Expression of the Ca_v Channels and Differentiation and Motility of Progenitors in FMRP-Deficient Neurospheres

(A) The proportion of cells responsive to glutamate receptor agonists (DHPG/KA/NMDA) in WT, *Fmr1* KO, and dMT NPCs at day 1 and 7 of differentiation (represented as number of cells responded/total number of cells). Each experimental group(n) = 5–8 and 3–5 neurospheres at days 1 and 7, respectively; responses of 75–100 cells were measured in each experiment.

(B) Representative images showing cells migrating out from the neurosphere at 0- and 24-hr time points. Neuron-like cells that moved freely outside the layer of radial glia are denoted as freely moving (fm) cells. Scale bar, 100 μm.

(C and D) Average speed of movement of fm cells at 12–24 hr (C) and 12–18 and 18–24 hr in neurospheres derived from WT, *Fmr1* KO, and dMT mice (D).

(E) The time each cell moved fast (rate >30 μm/hr, surges) divided by the time it moved slowly (rate <30 μm/hr, stalling) in WT, *Fmr1* KO, and dMT neurospheres at 12–18 hr of differentiation (represented as percent of control). WT(n) = 10, *Fmr1* KO(n) = 10, and dMT(n) = 8 neurospheres.

(F and G) The proportion of cells responsive to DHPG in the presence of $[Ca^{2+}]_e$ (F) and after withdrawal of $[Ca^{2+}]_e$ in WT, *Fmr1* KO, and dMT neurospheres (G).

(H–J) Representative single-cell responses to kainate (KA) and NMDA (H). The proportion of cells responsive to (I) KA and to (J) NMDA in WT, *Fmr1* KO, and dMT NPCs at day 7 of differentiation. Each group(n) = 3–5; responses of 75–100 cells were measured in each experiment. Data are expressed as means ± SEM. ***p < 0.001, **p < 0.01, *p < 0.05, one-way ANOVA with Tukey *post hoc* test (A, F, G, I, and J), chi-square statistics followed by Bonferroni *post hoc* test (C–E).

triggers a wide range of intracellular mechanisms, such as gene transcription and neurotransmitter release (Simms and Zamponi, 2014; Wheeler et al., 2012). L-type Ca_v channels are the key regulators of $[Ca^{2+}]_i$ and depolarization-induced Ca^{2+} influx into neurons is primarily mediated via these channels. Here we demonstrated a central role for Ca^{2+}-dependent mechanisms and increased Ca^{2+} influx through L-type Ca_v channels in altered differentiation of FXS NPCs. We showed that $[Ca^{2+}]_i$ responses to membrane depolarization were substantially augmented in both human and mouse FXS NPCs at the early stage of progenitor differentiation. The increased Ca^{2+} entry into NPCs via nifedipine-sensitive channels correlated with enhanced NPC differentiation and increased expression of the pore-forming α1 subunits of the L-type channels versus those of the T-type channels. Since Ca_v channel activity leads to increased BDNF expression, we investigated the effects of genetic reduction of BDNF expression on the altered

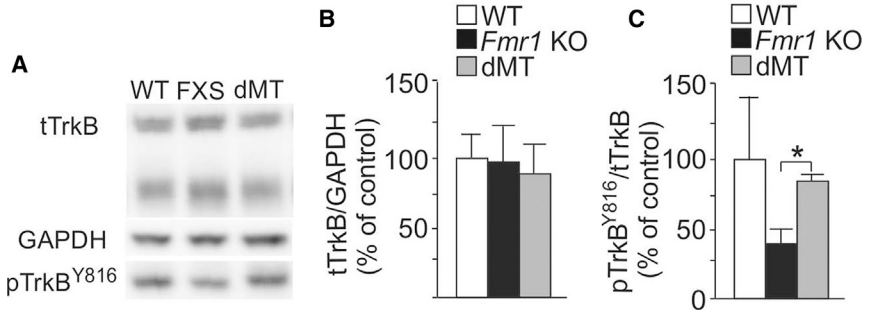

Figure 6. TrkB Phosphorylation in FMRP-Deficient NPCs

(A) Western blot image showing total TrkB (tTrkB), phosphorylated TrkB^{y816} (pTrkB), and GAPDH expression in WT, *Fmr1* KO, and dMT mouse neurospheres. A bar graph presenting optical density values showing (B) TrkB expression and (C) the increased phosphorylation of TrkB^{y816} in WT, *Fmr1* KO, and dMT NPCs. (n) = 4 per group. Data are expressed as means ± SEM. *$p < 0.05$ one-way ANOVA with Tukey *post hoc* test (B) and Student's t test (C). See also Figure S1.

differentiation of FXS NPCs. Reduced BDNF decreased the expression of the α subunits of both L- and T-type Ca_v channels and diminished $[Ca^{2+}]_i$ responses to depolarization. Both removal of $[Ca^{2+}]_e$ and reduced BDNF dampened enhanced responses to type I mGluR activation in FMRP-deficient mouse NPCs, suggesting that increased Ca^{2+} entry via L-type Ca_v channels facilitated mGluR5-signaling. BDNF-dependent mechanisms were involved in the regulation of calcium dynamics during differentiation, migration, and fate determination of FXS NPCs.

Inappropriate expression or dysregulation of Ca_v channels have been linked with various neurological disorders, including autism spectrum disorder (ASD), epilepsy, chronic pain, and migraine (Cain and Snutch, 2011; Pinggera et al., 2015; Strom et al., 2010). Two gain-of-function mutations in the genes encoding the $Ca_v1.3$ are associated with ASD (Pinggera et al., 2015). A gain-of-function phenotype of $Ca_v1.2$ is found in Timothy syndrome, which is characterized by lethal cardiac arrhythmia, immune deficiency, cognitive abnormalities, and autism (Splawski et al., 2004). Our present observations revealed that augmented Ca_v1 channel signaling in FMRP-deficient NPCs contributes to the pathophysiology of FXS that represents a clinically well-characterized variant of ASD. Most FXS individuals show at least some behavioral features of autism, and up to 60% of FXS males meet the diagnostic criteria of autism (Lozano et al., 2014). Our data suggest that mechanisms associated with activation of Ca_v channels could provide common molecular mechanisms leading to the autism phenotype in intellectual disability syndrome.

Both high-voltage activated (HVA) and low-voltage activated (LVA) Ca^{2+} channels are shown to be expressed in NPCs (D'Ascenzo et al., 2006; Lepski et al., 2013; Louhivuori et al., 2013). The mRNA expression of the pore-forming α1 subunits of all Ca_v channels was low in both human and mouse neurospheres at day 1 of differentiation. In mouse NPCs, we detected expression of the *Cacna1*, *Cacna1d*, and *Cacna1a* genes encoding HVA channels Cav1.2, Cav1.3, and Cav2.1, respectively, and the *Cacna1g* and *Cacna1h* genes encoding LVA channels Cav3.1 and Cav3.2, respectively. The subunit expression showed high variation, particularly in human NPCs. Although there was a tendency for an increase in *Cacna1c* and *Cacna1d* transcripts and a decrease in *Cacna1g* transcripts in mouse FXS NPCs, no significant differences in the expression of single subunits between FXS and their respective control NPCs were found. However, the ratio of the dihydropyridine-sensitive HVA Ca_v1/LVA Ca_v3 expression was increased. The FXS-specific change of Ca_v channel expression also existed in human iPSC-derived NPCs, which started to express less $Ca_v3.2$ during the first day of differentiation resulting in the increased ratio of Ca_v1/Ca_v3. There is evidence that Ca_v1 channels become more important as the neural cells mature; these results are consistent with enhanced differentiation of FXS NPCs. Reduced BDNF expression in FMRP-deficient NPCs decreased expression of both L- and T-type Ca_v channels and correlated with dramatically diminished $[Ca^{2+}]_i$ responses to depolarization.

According to the present data, augmentation of DHPG responses in FXS NPCs requires $[Ca^{2+}]_e$ and is facilitated by increased Ca^{2+} entry. Exaggerated group 1 mGluR function is a fundamental abnormality in FXS, and in *Fmr1*-KO mice mGluR-mediated long-term depression (LTD) is enhanced (Huber et al., 2002) and epileptiform discharges are prolonged (Chuang et al., 2005). Elevated responsiveness of FXS neurons associates with hyperarousal, sensory hypersensitivity, and susceptibility to epilepsy in the FXS phenotype (Lozano et al., 2014). By coupling Gq-type G-proteins, mGluR5 activates the PLC/inositol triphosphate receptor signaling pathway to mobilize $[Ca^{2+}]_i$ (Conn and Pin, 1997). The studies of Kim et al. (2018) showed that DHPG is not sufficient to activate PLC alone and local AMPA-mediated depolarization and Ca^{2+} influx via Ca_v1 channels are required to facilitate mGluR5-PLC cascades that underlie hippocampal mGluR-LTD. Both $Ca_v1.2$ and $Ca_v1.3$ are involved in glutamate-induced PLC activation, but $Ca_v1.2$ is the major isoform that interacts with mGluR5 and mediates L-type currents (Kato

et al., 2012). We observed that both isoforms contributed to the increased expression of L-type channels in FXS NPCs. Reduced BDNF decreased the expression of these Ca_v1 isoforms and substantially decreased Ca^{2+} influx in response to depolarization. However, given that mGluR5 signaling dictates the differentiation of NMDA-responsive cells from FXR NPCs (Achuta et al., 2017) and reduced BDNF promoted further differentiation of NMDA-responsive cells, reduced Ca^{2+} entry through L-type Ca_v channels in BDNF-deficient FXS NPCs was not sufficient to normalize the mGluR5-mediated alterations of FXS NPC differentiation.

$Ca_v1.2$ and $Ca_v1.3$ channels are often expressed in the same cell, but they differ in subcellular localization and coupling to the transcription machinery (Hasreiter et al., 2014). Their biophysical properties also differ and specific interacting proteins may selectively modulate each isoform (Wheeler et al., 2012). We found abnormal alternative splicing in the gene encoding calpastatin in human FXS NPCs. Calpastatin is an endogenous calpain inhibitor that can directly interact with the calmodulin binding site of the $Ca_v1.2$ isoform and reprime the channel function (Minobe et al., 2006; Sun et al., 2014). Calpain-calpastatin and calmodulin provide irreversible and reversible Ca^{2+}-activated systems, respectively, to control development, growth, and maintenance of cellular homeostasis (Murachi, 1983). We found that augmented responses to L-type Ca_v channel activation in FXS NPCs also correlated with enhanced motility of progenitors. There is evidence that L-type Ca_v channels regulate cell migration by promoting filopodia stability and maturation of focal adhesions through spatially restricted regulation of Ca^{2+} entry and subsequent activation of the protease calpain-1 (Jacquement et al., 2016). How alternative splicing of calpastatin affects the calpain-calpastatin system in FXS NPCs remains to be studied.

Signaling via Ca_v1 channels provides a mechanism to induce transcription of specific genes through changes of cytosolic and nuclear Ca^{2+}. Membrane depolarization induces via Ca_v1 channels transcriptional activation of the *BDNF* gene in cortical neurons (Tao et al., 1998). In particular, the $Ca_v1.2$ is implicated in transcriptional control of the *BDNF* gene. We showed previously that *BDNF* mRNA expression is increased in undifferentiated mouse FMRP-deficient NPCs and neurons (Louhivuori et al., 2011; Uutela et al., 2014). We did not observe any significant difference in the total *BDNF* mRNA expression between *Fmr1* KO and WT NPCs at day 1 of differentiation (data not shown) when activity-dependent responses were found to be increased in FXS NPCs. Reduced differentiation of cells expressing BDNF in FMRP-deficient neurospheres (Louhivuori et al., 2011) likely affected *BDNF* expression. In human NPCs, *BDNF* mRNA expression showed high variation and did not differ significantly between FXS and control NPCs. BDNF-mediated effects on fate determination of NPCs may contribute to diverse effects of reduced BDNF on the *Fmr1* KO mouse phenotype *in vivo* (Uutela et al., 2014). The phenotype of dMT differs substantially from that of the single deletion mutants of the *Bdnf* and *Fmr1* gene (Spencer et al., 2011). Altogether, the data suggest that the absence of FMRP may activate homeostatic mechanisms to compensate altered BDNF/TrkB signaling. In the brain of $Bdnf^{+/-}$ mice, TrkB autophosphorylation is reduced during early development (Di Lieto et al., 2012). The present study showed that the phosphorylation of the PLCγ1-binding tyrosine within the TrkB was increased to WT levels in dMT NPCs expressing less L-type channel subunits. The results are consistent with increased phosphorylation of TrkB, especially within the PLCγ1 site in the mouse prefrontal cortex and hippocampus after treatment with the blocker of the L-type channels (Koskimäki et al., 2015). Since the PLCγ docking site of TrkB is essential for hippocampal synaptic plasticity and acquisition of associative and spatial learning (Minichiello, 2009), reduced phosphorylation of the PLCγ site in FXS progenitors is in line with the impaired learning and plasticity defects in FXS. However, associative learning is highly impaired in dMT mice deficient of both FMRP and BDNF (Uutela et al., 2014), and the assessment of the consequences of altered responses of dihydropyridine-sensitive Ca_v channels in dMT NPCs for function of mature neurons and neuronal networks is complicated by probable compensatory mechanisms activated by reduced BDNF.

FXS is defined as a channelopathy, and direct interaction between FMRP and Ca_v2 channels indicates the role of N- and P/Q-type Ca_v channels in FXS (Ferron et al., 2014). The present studies demonstrated the important contribution of L-type Ca_v channels to the altered differentiation of FXS NPCs modeling molecular mechanisms disrupted in autism. Similar changes of Ca_v channel function and expression in human and mouse FXS neural progenitors confirmed the FXS specificity of our findings and highlighted the value of human iPSCs for further studies to explore correlations between functional *in vitro* findings and phenotypic features in FXS. Improved understanding of disordered developmental processes during early NPC differentiation may open possibilities for stem cell-based discovery of novel treatment options.

EXPERIMENTAL PROCEDURES

Mice

Fmr1 KO mice (B6.129P2-*Fmr1*$^{tml/Cgr}$/J) and $Bdnf^{+/-}$ mice (C57BL/6JOlaHsd) were purchased from Jackson Laboratory (Bar Harbor, ME) and maintained on the C57BL/6JOlaHsd substrain. $Fmr1^{+/-}$ female mice were crossed with male $Bdnf^{+/-}$ mice to generate

dMT mice, FXS, and WT littermates as described previously (Uutela et al., 2012). All animal experiments were performed in accordance with the guidelines of the Guide for the Care and Use of Laboratory Animals and European Economic Community Council Directive. The studies were approved by the Experimental Animal Ethics Committee of the National Laboratory Animal Center, Finland.

Mouse Cell Culture

NPCs were prepared from the WT, *Fmr1* KO, and dMT mice at E14 as described previously (Castrén et al., 2005). To induce neuronal differentiation, neurospheres (mid-sized 200–250-μm spheres) were plated on poly-DL-ornithine (Sigma)-coated cover glasses in culture medium without mitogens and differentiated for the indicated periods of time. The mitogens were added to cell cultures always a day before initiation of the differentiation.

Human iPSC Cultures

The research using human iPSCs was approved by the Ethical Committee of the Hospital District of Helsinki and Uusimaa. Written informed consent was provided to obtain human samples. We used four FXS iPSC lines (HEL100.1, HEL100.2, HEL69.5, and HEL70.3) and three control cell lines (HEL46.11, HEL23.3, and HEL11.4) and the protocol for their differentiation to neurospheres described previously (Achuta et al., 2018). Neurospheres (average size 200–250 μm) were differentiated for 1 day on poly-D-lysine/laminin (Sigma-Aldrich)-coated cover glasses in culture medium without mitogens.

Immunochemistry

Differentiated neurospheres were fixed with 4% paraformaldehyde in PBS (pH 7.4) for 10 min at room temperature (RT). Unspecific staining was blocked with 10% normal goat serum and 0.1% Triton X-100 in PBS for 45 min at RT, and followed by incubation with primary antibody recognizing microtubule-associated protein 2 and glutamate-aspartate transporter (both from Millipore; 1:500) at 4°C overnight. Secondary antibodies Alexa Fluor 488 (1:2,000, A11008; Invitrogen) and Alexa 568 (1:5,000, A11004; Invitrogen) were applied in PBS containing 1% BSA for 45 min at RT. After final washes, the cell nuclei were counterstained with Vectashield mounting media containing DAPI (Vector Laboratories). The fluorescent-stained differentiated NPCs were viewed and images were obtained with an LSM 5 Pascal laser scanning confocal microscope (Zeiss) and analyzed with the image analysis program ImageJ.

Intracellular Ca^{2+} Imaging

For calcium imaging experiments, 15 to 20 neurospheres were plated on coated cover glasses and differentiated for 1 and 7 days. The intracellular calcium recordings were performed as described previously (Achuta et al., 2018). Cells were challenged sequentially with glutamate receptor agonists at the following concentrations: DHPG (10 μM, Abcam Biochemicals); kainate (50 μM, Tocris Bioscience). Nifedipine (10 μM, Sigma) was used to block Ca_v1 channels.

Time-Lapse Imaging

For time-lapse imaging, a cell-culturing instrument combined with phase-contrast microscopy, automation, and environmental control (Cell-IQ, Chip-Man Technologies) was used. Neurospheres were plated on poly-DL-ornithine-coated six-well plates without mitogens. Cellular movement of adherent cells were monitored with an automated optics module controlled by machine vision-base firmware and analysis software during the first 24 hr of differentiation. The images were analyzed by an onboard Cell-IQ analyzer software package.

ELISA

BDNF expression was determined using BDNF ELISA (Quantikine human BDNF kit, R&D Systems) following the manufacturer's protocol. The cortical progenitors were homogenized in lysis buffer containing 137 mM NaCl, 20 mM Tris (pH 8.0), 1% (vol/vol) NP-40, 10% (vol/vol) glycerol, 50 mM sodium fluoride, 2× Complete Mini (Roche Diagnostics), and 2 mM sodium vanadate. Following homogenization, samples were incubated at 4°C for 20 min and centrifuged at 13,000 rpm for 15 min at 4°C. The total protein concentration was measured using a Bio-Rad DC protein assay (Bio-Rad), and the BDNF concentration was determined as pg/mL from the standard curve. To confirm the specificity of the ELISA kit, cell culture medium and lysis buffer without protein extract were used as negative controls.

Western Blotting

Proliferating mouse NPCs were collected and lysed in RIPA buffer supplemented with 1× protease and phosphatase inhibitor cocktail (Thermo Fisher Scientific) for western analysis. The total protein concentration was determined using a DC protein assay (Bio-Rad). Equal amounts of protein extracts (40 μg) were separated by SDS-PAGE under reducing conditions and transferred onto a polyvinylidene fluoride membrane (300 mA for 1 hr at 4°C) using a Trans-Blot Turbo System (Bio-Rad). The membranes were blocked in 3% BSA in Tris-buffered saline with Tween 20 (TBST) (pH 7.4) (0.1 M Tris, 0.15 M NaCl, and 0.1% Tween 20) at RT for 1 hr and incubated with the following primary antibodies: anti-TrkB (1:2,000; Transduction Laboratories) and anti-$TrkB^{Y816}$ (1:1,000; kind gift from Dr. M. Chao, Skirball Institute, NY, USA) at 4°C overnight. The membrane was washed three times with TBST and then incubated with horseradish-peroxidase-conjugated secondary antibody (1:10,000; GE Healthcare). Detection of immunoreactive proteins was performed using Pierce ECL western blotting substrates (Thermo Fisher Scientific) and visualized using a G:BOX Chemi XX6 imaging system (Syngene).

RNA Extraction and qRT-PCR

Total RNA was extracted from neural progenitors and mouse prefrontal cortex tissue using the RNA Purification Kit (Norgen Biotek) according to the manufacturer's instructions. cDNA was synthesized from 1 μg of RNA using the Transcriptor First Strand cDNA Synthesis kit (Roche). qRT-PCR was performed using SYBR Green I kit and a LightCycler 480 II Real-Time PCR System (Roche Diagnostics). The primers used to amplify the specific cDNA regions of transcripts are appended (Table S1). Each sample was run in triplicate with melting curve analysis to detect primer dimer artifacts. Data were analyzed using LightCycler 480 software (Roche) by the second derivative max method determining the threshold cycle (C_t). Relative quantities of the expression of

the α Ca_v subunits were calculated with the $\Delta\Delta C_t$ method (Livak and Schmittgen, 2001). Expression of *GAPDH* was used to normalize the data.

Microarray Analysis

The data for the transcriptome analysis using an Affymetrix Clariom D Human array (Thermo Fisher Scientific) have been deposited in NCBI's Gene Expression Omnibus (Achuta et al., 2018) and are accessible through accession number GEO: GSE103965). For the gene-level analysis, the raw expression data were normalized using the Expression Console program (v.1.3) (https://www.thermofisher.com/). The signal space transformation robust multi-array average method was used to normalize the data (Li and Wong, 2001). To identify differentially expressed genes, an empirical Bayes moderated t test was applied using the "limma" package (v.3.34.9) (Smyth, 2005). To address the problem of multiple testing, the p values were adjusted (Benjamini and Hochberg, 1995). A gene was considered differentially expressed if the adjusted p value was less than 0.05.

Alternative splicing analysis was performed using the transcriptome analysis console (TAC) (v.4.0) (https://www.thermofisher.com/). TAC was used with the default setting and only exon-level false discovery rate p values <0.05 were considered differentially expressed. The EventPointer (Romero et al., 2016) algorithm was used to detect splicing events and to test for significant differential splicing events.

Statistical Analysis

Data are expressed as means ± SEM. Statistical analysis was performed using Student's t test or one-way ANOVA with Tukey's HSD *post hoc* test and chi-square statistics with Bonferroni *post hoc* test. A p value <0.05 was considered statistically significant.

SUPPLEMENTAL INFORMATION

Supplemental Information includes one figure and one table can be found with this article online at https://doi.org/10.1016/j.stemcr.2018.11.003.

AUTHOR CONTRIBUTIONS

M.L.C. conceived and designed the experiments. C.D., U.-K.P., V.S.A., G.T., N.M., I.A., and V.R. performed the experiments. C.D., M.L.C., V.S.A., G.T., A.I., and V.A. analyzed the data. M.L.C., C.D., and V.S.A. wrote the manuscript.

ACKNOWLEDGMENTS

We are grateful to Outi Nikkilä for her help in mouse genotyping and Derek Ho for editing the text. This work was supported by grants from the Arvo and Lea Ylppö Foundation, the Päivikki and Sakari Sohlberg Foundation, the Finnish Medical Foundation, the Finnish Brain Research Foundation, and the Academy of Finland.

Received: March 26, 2018
Revised: November 2, 2018
Accepted: November 5, 2018
Published: November 29, 2018

REFERENCES

Achuta, V.S., Grym, H., Putkonen, N., Louhivuori, V., Karkkainen, V., Koistinaho, J., Roybon, L., and Castrén, M.L. (2017). Metabotropic glutamate receptor 5 responses dictate differentiation of neural progenitors to NMDA-responsive cells in fragile X syndrome. Dev. Neurobiol. *77*, 438–453.

Achuta, V.S., Moykkynen, T., Peteri, U.K., Turconi, G., Rivera, C., Keinänen, K., and Castrén, M.L. (2018). Functional changes of AMPA responses in human induced pluripotent stem cell-derived neural progenitors in fragile X syndrome. Sci. Signal. *11*. https://doi.org/10.1126/scisignal.aan8784.

Achuta, V.S., Rezov, V., Uutela, M., Louhivuori, V., Louhivuori, L., and Castrén, M.L. (2014). Tissue plasminogen activator contributes to alterations of neuronal migration and activity-dependent responses in fragile X mice. J. Neurosci. *34*, 1916–1923.

Benjamini, Y., and Hochberg, Y. (1995). Controlling the false discovery rate: a practical and powerful approach to multiple testing. J. R. Stat. Soc. B, 289–300.

Boland, M.J., Nazor, K.L., Tran, H.T., Szücs, A., Lynch, C.L., Paredes, R., Tassone, F., Sanna, P.P., Hagerman, R.J., and Loring, J.F. (2017). Molecular analyses of neurogenic defects in a human pluripotent stem cell model of fragile X syndrome. Brain *140*, 582–598.

Braun, K., and Segal, M. (2000). FMRP involvement in formation of synapses among cultured hippocampal neurons. Cereb. Cortex *10*, 1045–1052.

Cain, S.M., and Snutch, T.P. (2011). Voltage-gated calcium channels and disease. Biofactors *37*, 197–205.

Castrén, M., Tervonen, T., Kärkkäinen, V., Heinonen, S., Castrén, E., Larsson, K., Bakker, C., Oostra, B., and Åkerman, K. (2005). Altered neuronal differentiation of neural stem cells in fragile X syndrome. Proc. Natl. Acad. Sci. U S A *102*, 17834–17839.

Chuang, S.C., Zhao, W., Bauchwitz, R., Yan, Q., Bianchi, R., and Wong, R.K. (2005). Prolonged epileptiform discharges induced by altered group I metabotropic glutamate receptor-mediated synaptic responses in hippocampal slices of a fragile X mouse model. J. Neurosci. *25*, 8048–8055.

Conn, P.J., and Pin, J.P. (1997). Pharmacology and functions of metabotropic glutamate receptors. Annu. Rev. Pharmacol. Toxicol. *37*, 205–237.

Contractor, A., Klyachko, V.A., and Portera-Cailliau, C. (2015). Altered neuronal and circuit excitability in fragile X syndrome. Neuron *87*, 699–715.

D'Ascenzo, M., Piacentini, R., Casalbore, P., Budoni, M., Pallini, R., Azzena, G.B., and Grassi, C. (2006). Role of L-type Ca^{2+} channels in neural stem/progenitor cell differentiation. Eur. J. Neurosci. *23*, 935–944.

Darnell, J.C., Van Driesche, S.J., Zhang, C., Hung, K.Y., Mele, A., Fraser, C.E., Stone, E.F., Chen, C., Fak, J.J., Chi, S.W., et al. (2011). FMRP stalls ribosomal translocation on mRNAs linked to synaptic function and autism. Cell *146*, 247–261.

Di Lieto, A., Rantamaki, T., Vesa, L., Yanpallewar, S., Antila, H., Lindholm, J., Rios, M., Tessarollo, L., and Castren, E. (2012). The responsiveness of TrkB to BDNF and antidepressant drugs is

differentially regulated during mouse development. PLoS One *7*, e32869.

Dolphin, A.C. (2016). Voltage-gated calcium channels and their auxiliary subunits: physiology and pathophysiology and pharmacology. J. Physiol. *594*, 5369–5390.

Ferron, L., Nieto-Rostro, M., Cassidy, J.S., and Dolphin, A.C. (2014). Fragile X mental retardation protein controls synaptic vesicle exocytosis by modulating N-type calcium channel density. Nat. Commun. *5*, 3628.

Gonçalves, J.T., Anstey, J.E., Golshani, P., and Portera-Cailliau, C. (2013). Circuit level defects in the developing neocortex of fragile X mice. Nat. Neurosci. *16*, 903–909.

Hasreiter, J., Goldnagl, L., Böhm, S., and Kubista, H. (2014). Cav1.2 and Cav1.3 L-type calcium channels operate in a similar voltage range but show different coupling to Ca(2+)-dependent conductances in hippocampal neurons. Am. J. Physiol. Cell Physiol. *306*, C1200–C1213.

Huber, K.M., Gallagher, S.M., Warren, S.T., and Bear, M.F. (2002). Altered synaptic plasticity in a mouse model of fragile X mental retardation. Proc. Natl. Acad. Sci. U S A *99*, 7746–7750.

Jacquement, G., Baghirov, H., Georgiadou, M., Sihto, H., Peuhu, E., Cettour-Janet, P., He, T., Perälä, M., Kronqvist, P., Joensuu, H., et al. (2016). L-type calcium channel regulate filopodia stability and cancer cell invasion downstream of integrin signalling. Nat. Commun. *7*, 13297.

Jansson, L.C., Louhivuori, L., Wigren, H.K., Nordstrom, T., Louhivuori, V., Castren, M.L., and Akerman, K.E. (2012). Brain-derived neurotrophic factor increases the motility of a particular N-methyl-D-aspartate/GABA-responsive subset of neural progenitor cells. Neuroscience *224*, 223–234.

Kato, H.K., Kassai, H., Watabe, A.M., Aiba, A., and Manabe, T. (2012). Functional coupling of the metabotropic glutamate receptor, InsP3 receptor and L-type Ca^{2+} channel in mouse CA1 pyramidal cells. J. Physiol. *590* (Pt 13), 3019–3034.

Kim, H.H., Lee, K.H., Lee, D., Han, Y.E., Lee, S.H., Sohn, J.W., and Ho, W.K. (2015). Costimulation of AMPA and metabotropic glutamate receptors underlies phospholipase C activation by glutamate in hippocampus. J. Neurosci. *35*, 6401–6412.

Kim, J.W., Park, K., Kang, R.J., Gonzales, E.L.T., Kim, D.G., Oh, H.A., Seung, H., Ko, M.J., Kwon, K.J., Kim, K.C., et al. (2018). Pharmacological modulation of AMPA receptor rescues social impairments in animal models of autism. Neuropsychopharmacology https://doi.org/10.1038/s41386-018-0098-5.

Kooy, R.F., D'Hooge, R., Reyniers, E., Bakker, C.E., Nagels, G., De Boulle, K., Storm, K., Clincke, G., De Deyn, P.P., Oostra, B.A., et al. (1996). Trangenic mouse model for the fragile X syndrome. Am. J. Med. Genet. *64*, 241–245.

Koskimäki, J., Matsui, N., Umemori, J., Rantamaki, T., and Castrén, E. (2015). Nimodipine activates TrkB neurotrophin receptors and induces neuroplastic and neuroprotective signaling events in the mouse hippocampus and prefrontal cortex. Cell. Mol. Neurobiol. *35*, 189–196.

La Fata, G., Gartner, A., Dominguez-Iturza, N., Dresselaers, T., Dawitz, J., Poorthuis, R.B., Averna, M., Himmelreich, U., Meredith, R.M., Achsel, T., et al. (2014). FMRP regulates multipolar to bipolar transition affecting neuronal migration and cortical circuitry. Nat. Neurosci. *17*, 1693–1700.

Lepski, G., Jannes, C.E., Nikkhah, G., and Bischofberger, J. (2013). cAMP promotes the differentiation of neural progenitor cells in vitro via modulation of voltage-gated calcium channels. Front. Cell Neurosci. *7*, 155.

Li, C., and Wong, W.H. (2001). Model-based analysis of oligonucleotide arrays: expression index computation and outlier detection. Proc. Natl. Acad. Sci. U S A *98*, 31–36.

Livak, K.J., and Schmittgen, T.D. (2001). Analysis of relative gene expression data using real-time quantitative PCR and the 2(-Delta Delta C(T)) method. Methods *25*, 402–408.

Louhivuori, L., Louhivuori, V., Wigren, H.K., Hakala, E., Castrén, M.L., and Åkerman, K.E. (2013). Role of low voltage activated calcium channels in neuritogenesis and proliferation of embryonic neural stem cells. Stem Cells Dev. *22*, 1206–1219.

Louhivuori, V., Vicario, A., Uutela, M., Rantamäki, T., Louhivuori, L.M., Castrén, E., Tongiorgi, E., Akerman, K.E., and Castrén, M.L. (2011). BDNF and TrkB in neuronal differentiation of Fmr1-knockout mouse. Neurobiol. Dis. *41*, 469–480.

Lozano, R., Rosero, C.A., and Hagerman, R.J. (2014). Fragile X spectrum disorders. Intractable Rare Dis. Res. *3*, 134–146.

Minichiello, L. (2009). TrkB signalling pathways in LTP and learning. Nat. Rev. Neurosci. *10*, 850–860.

Minobe, E., Hao, L.Y., Saud, Z.A., Xu, J.J., Kameyama, A., Maki, M., Jewell, K.K., Parr, T., Bardsley, R.G., and Kameyama, M. (2006). A region of calpastatin domain L that reprimes cardiac L-type Ca2+ channels. Biochem. Biophys. Res. Commun. *348*, 288–289.

Murachi, T. (1983). Calpain and calpastatin. Trends Biochem. Sci. *8*, 167–169.

Pinggera, A., Lieb, A., Benedetti, B., Lampert, M., Monteleone, S., Liedl, K.R., Tuluc, P., and Striessnig, J. (2015). CACNA1D de novo mutations in autism spectrum disorders activate Cav1.3 L-type calcium channels. Biol. Psychiatry *77*, 816–822.

Platel, J.C., Dave, K.A., and Bordey, A. (2008). Control of neuroblast production and migration by converging GABA and glutamate signals in the postnatal forebrain. J. Physiol. *586*, 3739–3743.

Romero, J.P., Muniategui, A., De Miguel, F.J., Aramburu, A., Montuenga, L., Pio, R., and Rubio, A. (2016). EventPointer: an effective identification of alternative splicing events using junction arrays. BMC Genomics *17*, 467.

Rosenberg, S.S., and Spitzer, N.C. (2011). Calcium signaling in neuronal development. Cold Spring Harb. Perspect. Biol. *3*, a004259.

Simms, B.A., and Zamponi, G.W. (2014). Neuronal voltage-gated calcium channels: structure, function, and dysfunction. Neuron *82*, 24–45.

Smyth, G.K. (2005). Limma: linear models for microarray data. In Bioinformatics and Computational Biology Solutions Using R and Bioconductor, R. Gentleman, V. Carey, S. Dudoit, R. Irizarry, and W. Huber, eds. (Springer), pp. 397–420.

Spencer, C., Alekseyenko, O., Hamilton, S., Thomas, A., Serysheva, E., Yuva-Paylor, L.A., and Paylor, R. (2011). Modifying behavioral

phenotypes in Fmr1KO mice: genetic background differences reveal autistic-like responses. Autism Res. *4*, 40–56.

Splawski, I., Timothy, K.W., Sharpe, L.M., Decher, N., Kumar, P., Bloise, R., Napolitano, C., Schwartz, P.J., Joseph, R.M., Condouris, K., et al. (2004). Ca(V)1.2 calcium channel dysfunction causes a multisystem disorder including arrhythmia and autism. Cell *119*, 19–31.

Strom, S.P., Stone, J.L., Ten Bosch, J.R., Merriman, B., Cantor, R.M., Geschwind, D.H., and Nelson, S.F. (2010). High-density SNP association study of the 17q21 chromosomal region linked to autism identifies CACNA1G as a novel candidate gene. Mol. Psychiatry *15*, 996–1005.

Sun, W., Feng, R., Hu, H., Guo, F., Gao, Q., Shao, D., Yin, D., Wang, H., Sun, X., Zhao, M., et al. (2014). The Ca(2+)-dependent interaction of calpastatin domain L with the C-terminal tail of the Cav1.2 channel. FEBS Lett. *588*, 665–671.

Tao, X., Finkbeiner, S., Arnold, D.B., Shaywitz, A.J., and Greenberg, M.E. (1998). Ca^{2+} influx regulates BDNF transcription by a CREB family transcription factor-dependent mechanism. Neuron *20*, 709–726.

Telias, M., Kuznitsov-Yanovsky, L., Segal, M., and Ben-Yosef, D. (2015). Functional deficiencies in fragile X neurons derived from human embryonic stem cells. J. Neurosci. *35*, 15295–15306.

Tervonen, T.A., Louhivuori, V., Sun, X., Hokkanen, M.E., Kratochwil, C.F., Zebryk, P., Castrén, E., and Castrén, M.L. (2009). Aberrant differentiation of glutamatergic cells in neocortex of mouse model for fragile X syndrome. Neurobiol. Dis. *33*, 250–259.

Uutela, M., Lindholm, J., Louhivuori, V., Wei, H., Louhivuori, L.M., Pertovaara, A., Akerman, K., Castrén, E., and Castrén, M.L. (2012). Reduction of BDNF expression in *Fmr1* knockout mice worsens cognitive deficits but improves hyperactivity and sensorimotor deficits. Genes Brain Behav. *11*, 513–523.

Uutela, M., Lindholm, J., Rantamäki, T., Umemori, J., Hunter, K., Voikar, V., and Castrén, M.L. (2014). Distinctive behavioral and cellular responses to fluoxetine in the mouse model for fragile X syndrome. Front Neurosci. *8*, 150.

Verkerk, A.J., Pieretti, M., Sutcliffe, J.S., Fu, Y.H., Kuhl, D.P.A., Pizzuti, A., Reiner, O., Richards, S., Victoria, M.F., Zhang, F., et al. (1991). Identification of a gene (FMR-1) containing a CGG repeat coincident with breakpoint cluster region exhibiting length variation in fragile X syndrome. Cell *65*, 905–914.

Wheeler, D.G., Groth, R.D., Ma, H., Barrett, C.F., Owen, S.F., Safa, P., and Tsien, R.W. (2012). Ca(V)1 and Ca(V)2 channels engage distinct modes of Ca(2+) signaling to control CREB-dependent gene expression. Cell *149*, 1112–1124.

Zheng, F., Zhou, X., Luo, Y., Xiao, H., Wayman, G., and Wang, H. (2011). Regulation of brain-derived neurotrophic factor exon IV transcription through calcium responsive elements in cortical neurons. PLoS One *6*, e28441.

Zheng, J.Q., and Poo, M.M. (2007). Calcium signaling in neuronal motility. Annu. Rev. Cell Dev. Biol. *23*, 375–404.